

## Article

# Research on the Morphology, Electro-Optical Properties and Mechanical Properties of Electrochromic Polymer-Dispersed Liquid Crystalline Films Doped with Anthraquinone Dyes

Chenghu Zhao <sup>1</sup>, Yongchuan Hu <sup>1</sup>, Jianjun Xu <sup>2,3</sup>, Meina Yu <sup>1</sup> , Cheng Zou <sup>1,3</sup>, Qian Wang <sup>1,\*</sup>, Yanzi Gao <sup>1,\*</sup>   
and Huai Yang <sup>1,3,4,\*</sup>

<sup>1</sup> Institute for Advanced Materials and Technology, University of Science and Technology Beijing, Beijing 100083, China

<sup>2</sup> School of Materials Science and Engineering, University of Science and Technology Beijing, Beijing 100083, China

<sup>3</sup> Beijing Advanced Innovation Center for Materials Genome Engineering, University of Science and Technology Beijing, Beijing 100083, China

<sup>4</sup> School of Materials Science and Engineering, Peking University, Beijing 100083, China

\* Correspondence: b2286713@ustb.edu.cn (Q.W.); gaoyanzi@ustb.edu.cn (Y.G.); yanghuai@pku.edu.cn (H.Y.)

**Abstract:** In this paper, dye-doped polymer-dispersed liquid crystalline (DDPDLC) films were prepared with high mechanical properties and low driving voltage by doping different dichroic anthraquinone dyes. The effects of various dye and doping concentrations on microscopic morphology, electro-optical characteristics, and mechanical characteristics were investigated. The optimal doping concentrations of different dyes were also explored. The results show that the addition of all dyes decreased the contrast ratio (CR) and the transmittance and mechanical properties of the polymer-dispersed liquid crystalline (PDLC) films. Similar mechanisms underlie the effects of solvent red 111 and solvent blue 104, which lower the driving voltages of the PDLC films. With the increasing concentration of the dye, the haze of the films first decreased and then increased after the content of the dye reached a certain level. For PDLC films doped with solvent green 28, the driving voltage and haze increased with the increasing content of the dye. According to different influencing factors, the dye content corresponding to the best performance of solvent red 111, solvent green 28 and solvent blue 104 is 0.8 wt%, 2.0 wt% and 0.3 wt%. Electrochromic PDLC films have been prepared based on the research results of dye content. The mechanical properties, electro-optical properties and microstructures of the films have been studied. The results show that the DDPDLC films could change color by tuning the applied voltages. The research provides a theoretical basis for obtaining PDLC films with a wider color gamut and supports the practical application of visible light camouflage technology in the military.

**Keywords:** polymer-dispersed liquid crystal; dye-doped polymer-dispersed liquid crystal; electro-optical properties; mechanical properties; gamut range



**Citation:** Zhao, C.; Hu, Y.; Xu, J.; Yu, M.; Zou, C.; Wang, Q.; Gao, Y.; Yang, H. Research on the Morphology, Electro-Optical Properties and Mechanical Properties of Electrochromic Polymer-Dispersed Liquid Crystalline Films Doped with Anthraquinone Dyes. *Crystals* **2023**, *13*, 735. <https://doi.org/10.3390/cryst13050735>

Academic Editor: Jeroen Beeckman

Received: 27 March 2023

Revised: 12 April 2023

Accepted: 17 April 2023

Published: 27 April 2023



**Copyright:** © 2023 by the authors. Licensee MDPI, Basel, Switzerland. This article is an open access article distributed under the terms and conditions of the Creative Commons Attribution (CC BY) license (<https://creativecommons.org/licenses/by/4.0/>).

## 1. Introduction

Camouflage is the instinct of natural creatures to protect themselves [1,2]. Rapid advances in detection technology in modern warfare threaten the concealment capability of military operations, which has an impact on national military security [3–5]. The camouflage techniques commonly used in the military today often use nets and patterns of fixed colors and geometric shapes covered or painted on the target surface to achieve camouflage effects [6], including camouflage clothing [7,8], surface filming [9,10] etc. These camouflage methods can only be effective when the objective is not moving or moving slowly and are prone to failure in the mobile environment of real-time [11]. By adjusting the material properties [12,13] and altering the color [14], it may accurately and sensitively

real-time dynamic react to changes in the surrounding environment, avoiding detection technology tracking and enhancing the security of military operations. Electrochromic materials are considered to be one of the promising research directions in the field of visible light camouflage technology for several applications, such as smart windows [15], smart displays [16–19] and optical lenses [20]. However, the current electrochromic materials have short lifespans, single color change and strong monochromaticity, which restrict their large-scale use, and it is urgent to develop a new electrochromic material to solve the above problems.

Polymer-dispersed liquid crystalline (PDLC) is a dimming film with a mesh structure formed by dispersing liquid crystal materials in the form of droplets in a polymer matrix, which has the unique property of transmitting when voltage is applied and scattering when voltage is removed [21–24]. It has both the optical response characteristics of liquid crystals and the flexible large-area production and good mechanical processing characteristics of polymers and is widely used in smart windows [17,18,25,26], flexible displays [27,28], electro-optical switches [29] and micro lenses [30]. However, to realize their application in visible stealth technology, it is necessary to be able to have a clear switch between different colors, for example, to realize the rapid switch between military camouflage in forest terrain (green) and desert-type (sandy soil) environments. Therefore, it is essential to give PDLC films a color-changing ability, and it is vital to broaden the color ranges and improve the color richness of PDLC films without affecting the mechanical and electro-optical properties of the PDLC films.

The use of dichroic dyes in liquid crystal color change products has been a very popular research area in recent years and has considerable development prospects [31–36]. Fluorescent dichroic dyes can have very multi-way color changes through the design of the molecular structure [37] and can also be used to obtain various colors through the blending of different dyes [38]. Nowadays, azo dyes [35,39,40] and anthraquinone dyes [41–44] are the primary substances utilized for dichroic dyes in PDLC films. The doping studies of the above dyes have improved the performance of PDLC in different aspects, but there are limitations to the study of its color richness.

This study adopts the previously reported PDLC film with high mechanical properties and excellent electro-optical properties [45] and further optimizes the ratio of the above-mentioned PDLC film components by doping them with different colors of dichroic anthraquinone dyes. DDPDLC films were prepared using the polymerization-induced phase separation (PIPS) method [46], and the effects of the kind of dyes and their doping concentrations on the structure and properties of color-changing PDLC films were investigated. On the one hand, it reveals the effects of the kind of dyes and its doping concentrations on PDLC network morphology, electro-optical properties, haze, transmittance, and mechanical properties to help obtain PDLC film with excellent performance; on the other hand, the contribution of dye species to the color gamut range of PDLC films is discussed. The color gamut range is an important parameter in the display field, which can provide a theoretical basis for obtaining color-changing PDLC films with a wider color gamut and support the subsequent practical application in visible light camouflage technology.

## 2. Experimental

### 2.1. Materials

The nematic liquid crystals (LC) E8 ( $n_0 = 1.527$ ,  $n_e = 1.774$ ,  $T_{C-N} < 233.15$  K,  $T_{N-I} = 345.2$  K, Jiangsu Hecheng Display Technology Co., Ltd., Nanjing, China). The monomers, isobornyl acrylate (IBOA), acrylic acid hexyl ester (HA), and the crosslinking agent 1,4-butanediol diacrylate (BDDA) were acquired at Beijing InnoChem Science & Technology Co., Ltd. The UV photoinitiator Irgacure 651 was provided by Shanghai Macklin Biochemical Co., Ltd., P. R. China. The chemicals used in this paper were used directly without further purification, and their structural formulas are depicted in Figure 1.

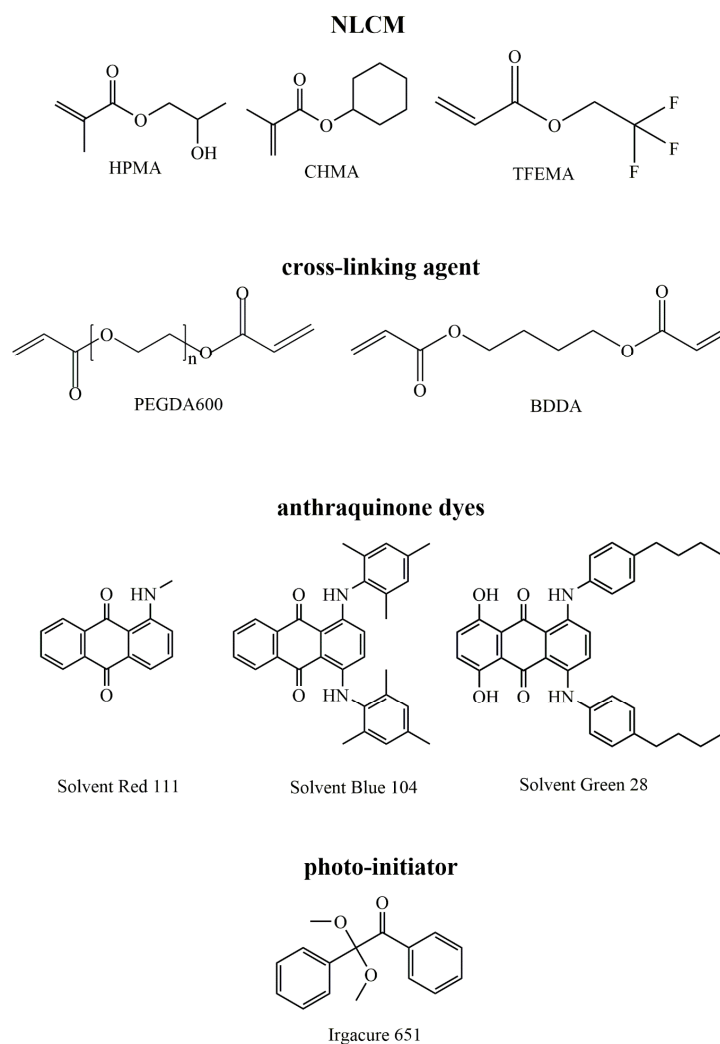


**Figure 1.** The chemical structures of the materials used.

## 2.2. Sample Preparation

Based on the PDLC film with excellent electro-optical properties prepared by Hu et al. [45], we doped three dichroic anthraquinone dyes into the PDLC during the preparation process and used the PIPS method to prepare the dye-doped polymer-dispersed liquid crystalline (DDPDLC) film.

First of all, liquid crystals, anthraquinone dyes, monomers and photo-initiators are uniformly mixed in certain proportions, as listed in Table 1. After filtering, the mixture is stirred with a magnetic stirrer for 10 min. The mixture is then poured into the middle of the conductive film between the two rollers of the laminating machine, and the two rollers are reversed to extrude the film. Finally, the film is placed in a UV curing oven and cured with UV light (365 nm) at a light intensity of 6 mW/cm<sup>2</sup> for 7 min.

**Table 1.** Chemical composition and weight ratio of the samples.

Sample	Content (wt%)		
	CHMA/IBMA/HPMA/ TFEMA/BDDA/PEGDA600	Dye	E8
Group A A0	18.0/6.0/6.4/1.6/1.6/6.4	Solvent Red 111 0	60

Table 1. Cont.

Sample	Content (wt%)		
	CHMA/IBMA/HPMA/ TFEMA/BDDA/PEGDA600	Dye	E8
A1	18.0/6.0/6.4/1.6/1.6/6.4	0.3	60
A2	18.0/6.0/6.4/1.6/1.6/6.4	0.5	60
A3	18.0/6.0/6.4/1.6/1.6/6.4	0.8	60
A4	18.0/6.0/6.4/1.6/1.6/6.4	1.0	60
A5	18.0/6.0/6.4/1.6/1.6/6.4	1.5	60
A6	18.0/6.0/6.4/1.6/1.6/6.4	2.0	60
Group B		Solvent Green 28	
A0	18.0/6.0/6.4/1.6/1.6/6.4	0	60
B1	18.0/6.0/6.4/1.6/1.6/6.4	0.3	60
B2	18.0/6.0/6.4/1.6/1.6/6.4	0.5	60
B3	18.0/6.0/6.4/1.6/1.6/6.4	0.8	60
B4	18.0/6.0/6.4/1.6/1.6/6.4	1.0	60
B5	18.0/6.0/6.4/1.6/1.6/6.4	1.5	60
B6	18.0/6.0/6.4/1.6/1.6/6.4	2.0	60
Group C		Solvent Blue 104	
A0	18.0/6.0/6.4/1.6/1.6/6.4	0	60
C1	18.0/6.0/6.4/1.6/1.6/6.4	0.3	60
C2	18.0/6.0/6.4/1.6/1.6/6.4	0.5	60
C3	18.0/6.0/6.4/1.6/1.6/6.4	0.8	60
C4	18.0/6.0/6.4/1.6/1.6/6.4	1.0	60
C5	18.0/6.0/6.4/1.6/1.6/6.4	1.5	60
C6	18.0/6.0/6.4/1.6/1.6/6.4	2.0	60

### 2.3. Characterizations

#### 2.3.1. Absorption Analysis

Ultraviolet-Visible Infrared (UV-Vis-IR) spectrophotometer (Lambda 35, Perkin Elmer, Waltham, MA, USA) is used for the absorption spectroscopy of the samples, the dichroism of the dyes, and the haze and transmittance analysis of the PDLC films.

The ordering parameters, dichroic ratio, dissolvability and photostability are the main performance parameters for dichroic dyes and are mainly determined by the structure and properties of the dye.

The equations for the ordering parameters and the dichroic ratio of the dichroic dyes [47] are as follows:

$$S_A = \frac{A_{//} - A_{\perp}}{A_{//} + 2A_{\perp}} \quad (1)$$

$$R_A = \frac{A_{//}}{A_{\perp}} \quad (2)$$

where  $A_{//}$  and  $A_{\perp}$  are the absorbance of the dye in the parallel and perpendicular liquid crystal pointing sagittal directions under polarized light, respectively.  $S_A$  and  $R_A$  represent the ordering parameters and the dichroic ratio, respectively.

#### 2.3.2. Morphological Analysis

The cured DDPDLC film samples were cut into long strips, and the strips were immersed in a beaker containing cyclohexane solvent for a fortnight under normal atmospheric temperature, with the liquid crystal molecules and unpolymerized polymeric monomers dissolved in the solvent to remove the liquid crystal monomers from the polymer network. The solvent was changed every two days, and the strips were then removed and placed in an oven at 333.15 K and dried under vacuum for 24 h. The surface was then sprayed with gold. The morphology and dimensions information of the samples were observed by scanning electron microscopy (SEM, HITACHI S-4800).

### 2.3.3. Morphological Analysis

Electro-optical properties were measured by a liquid crystal device parameters tester (LCT-5016C, Changchun Liancheng Instrument Co. Ltd., Changchun, China), which used a halogen laser beam ( $\lambda = 560.0$  nm) as the incident light source. The sample transmittance was recorded by a photodiode, and then the response of the photodiode was monitored with a digital storage oscilloscope (DSO); the distance between the sample and the detector was about 300 mm. In this study, the external electric field was the frequency (1 kHz) adjustable square wave electric field, the experiments involved were carried out at room temperature, and the transmittance of air was normalized to 100%. The main electro-optical parameters obtained with this instrument are mainly transmittance, threshold and saturation voltages, contrast ratio and response time. Threshold and saturation voltages were denoted by  $V_{th}$  and  $V_{sat}$ , which represented the voltage required for the transmittance to increase to 10% and 90% of the maximum on-state transmittance ( $T_{on}$ ), separately. Contrast ratio (CR) was defined as the ratio of on-state transmittance ( $T_{on}$ ) to the off-state transmittance ( $T_{off}$ ). The response time included the rising time ( $t_{on}$ ) and falling time ( $t_{off}$ ), which represented that the time needed for the transmittance increased from 10% to 90% and decreased from 90% to 10% of  $T_{on}$ , separately. The intensity of incident light was assumed to be 100% transmittance.

### 2.3.4. Mechanical Properties Analysis

The shear strength of all of the PDLC film samples was tested using a mechanical ductile testing machine (LETRY) at a tensile rate of 5 mm/min. Similar to the LC cell, the glass substrates were replaced with two transparent ITO-coated PET films. For the test samples, the effective area was 2 cm  $\times$  2 cm, and the film thickness was 20  $\mu$ m, which was controlled by adding 0.5 wt% of 20  $\mu$ m glass beads.

## 3. Results and Discussion

### 3.1. The Characterization of the Dichroism of Anthraquinone Dyes by UV Visible Polarized Absorption Spectroscopy

As shown in Figure 2a, the fundamental characterization of the employed dyes was carried out using a UV spectrophotometer with ethanol as the solvent. The absorption spectra of solvent red 111, solvent green 28, and solvent blue 104 showed that the red anthraquinone dye had a narrow absorption range with the maximum absorption wavelength at 500 nm, the green anthraquinone dye had strong absorption peaks from 630 nm to 710 nm, and the blue anthraquinone dye also had strong absorption peaks from 560 nm to 650 nm.

The ordering parameters and the dichroic ratio of dichroic dyes are often used to evaluate the practical value of dichroic dyes. Figure 2b–d represent the UV-Vis polarized absorption spectra characterization of the dichroism of three anthraquinone dyes in solvent red 111, solvent green 28 and solvent blue 104, and the graph shows that the values of absorbance  $A_{\parallel}$  and  $A_{\perp}$  of solvent red 111 dye in parallel and perpendicular liquid crystal pointing sagittal directions under polarized light are 0.40 and 0.09, while  $A_{\parallel}$  and  $A_{\perp}$  for solvent green 28 dye and solvent blue 104 dyes were 0.34 and 0.10, 0.12 and 0.44, respectively. The ordering parameters ( $S_A$ ) of the three dyes can be calculated from Equation (1) as 0.53, 0.44, and 0.47, respectively. The dichroic ratio ( $R_A$ ) of the three dyes can be obtained from Equation (2) as 4.45, 3.40, and 3.70, respectively.

Generally, the ordering parameter  $S_A$  for positive dyes ranges from  $0 < S_A < 1$ , and  $S_A$  for negative dyes ranges from  $-0.5 < S_A < 0$ . The dyes selected in the paper are within the range and have practical value. The dichroism size is related to the linear structure of the dyes (length, width, dipole moment, etc.), the linear length and diameter of solvent green 28 dyes and solvent blue 104 dyes are smaller compared to solvent red 111 dyes, so the ordering parameter and dichroism ratio are smaller compared to solvent red 111 dyes, but still have practical value.

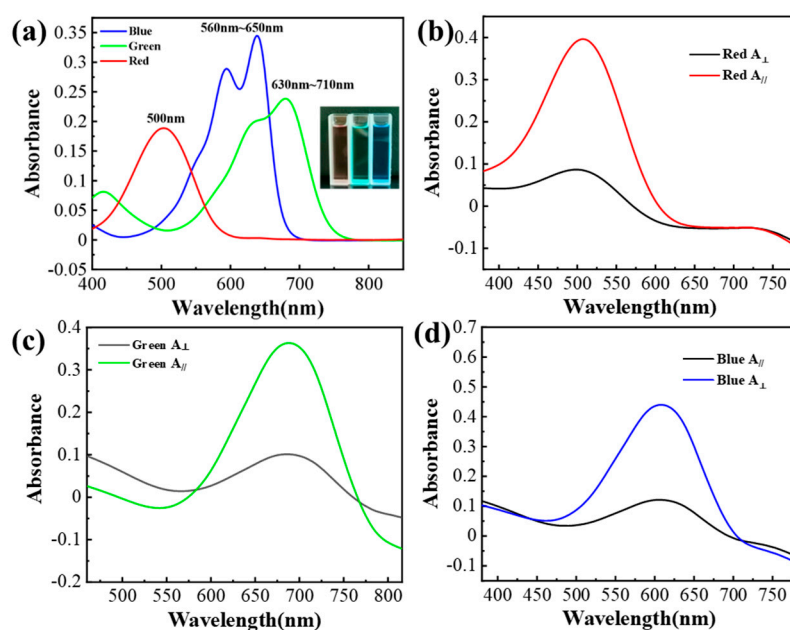


**Figure 2.** The absorption spectra of anthraquinone dye: (a) Fundamental characteristics of dyes; (b) solvent red 111; (c) solvent green 28; (d) solvent blue 104.

### 3.2. Effect of Different Dyes and Their Doping Contents on the Morphology of PDLC Dimming Films

To examine the impact of dye concentration on the microscopic morphology of PDLC films, different anthraquinone dyes with concentrations of 0.3 wt%, 0.5 wt%, 0.8 wt%, 1.0 wt%, 1.5 wt%, and 2.0 wt% were doped into the optimal PDLC film. The detailed formulation is shown in Table 1.

Figures 3 and 5 show the SEM morphology of the pure PDLC film samples, and the PDLC film samples doped with different concentrations of solvent red 111 and solvent blue 104. As can be seen from the picture, the surface of pure PDLC films was uniformly distributed and morphologically intact; therefore, different dye doping concentrations have certain effects on the mesh size and network distribution of the polymer matrix. The trend of the effect of dye concentration change on the morphology of the network is basically the same in Figures 3 and 5, and with the increasing dye concentration, the mesh size becomes larger [48,49]. This phenomenon can be explained by the fact that in pure PDLC, the phase separation is faster, and the viscosity of the system increases rapidly as the polymerization continues [50,51], which makes the gathering of liquid crystal molecules more difficult, so the liquid crystal microdroplet size is smaller. Additionally, after the introduction of dyes, the dye molecules absorb some UV light needed for polymerization, which makes the actual light intensity energy involved in polymerization decrease, and the polymerization rate descends, thus the liquid crystal molecules have sufficient time to diffuse and gather, so the liquid crystal microdroplet size and the polymer matrix mesh size becomes larger.

Figure 4 shows the SEM morphology of the pure PDLC film sample and the PDLC film sample doped with different concentrations of solvent green 28. The microscopic morphology shows that the polymer mesh size decreases with increasing concentration of solvent green 28 dye, and the mesh distribution becomes increasingly dense. This is due to the relatively large molecular mass of solvent green 28, which leads to a smaller mesh size because fewer dye molecules are doped with the same mass fraction and faster polymerization rate compared to doping with solvent red 111 and solvent blue 104.

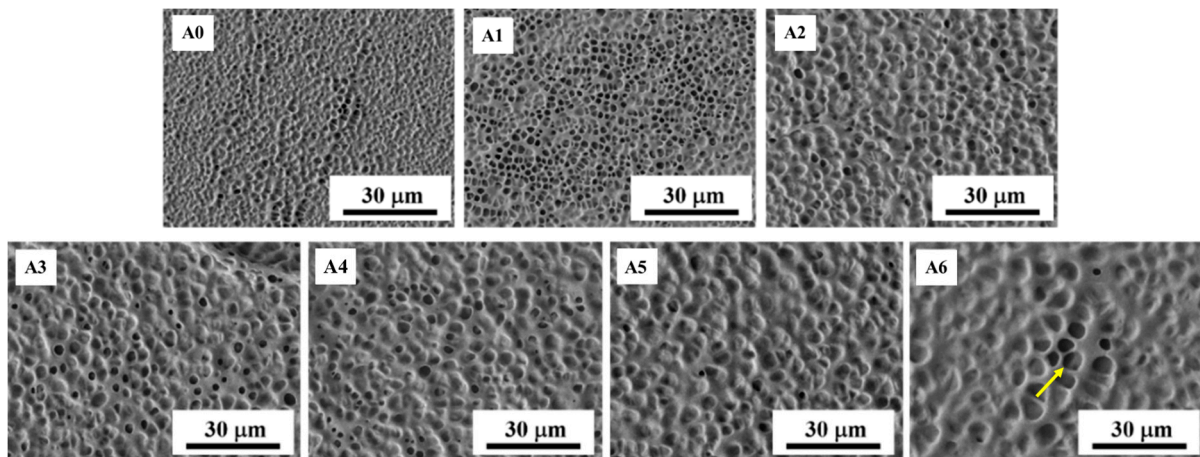


**Figure 3.** Microscopic morphology of PDLC doped with different concentrations of solvent red 111: (A0) 0 wt%; (A1) 0.3 wt%; (A2) 0.5 wt%; (A3) 0.8 wt%; (A4) 1.0 wt%; (A5) 1.5 wt%; (A6) 2.0 wt%. (The arrow points to the mesh of PDLC films.)

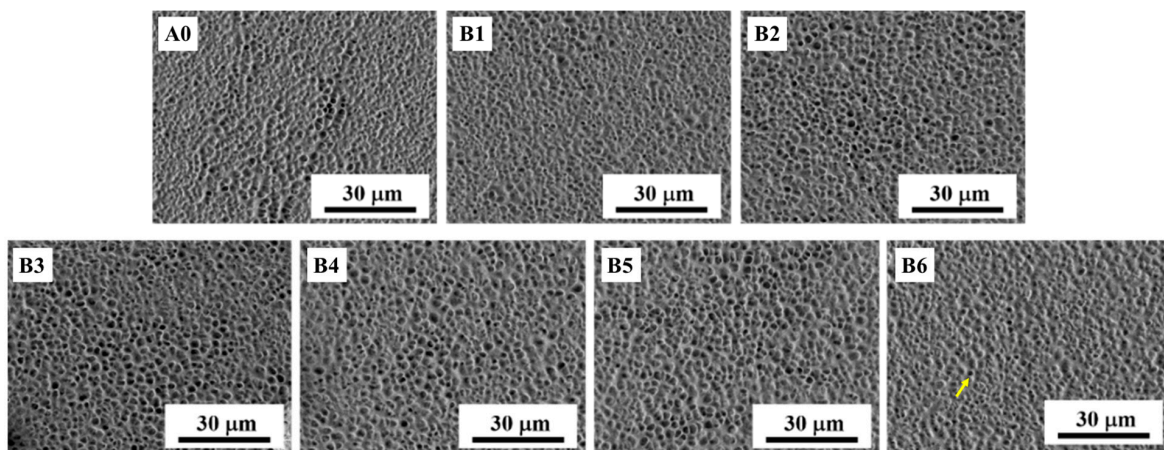


**Figure 4.** Microscopic morphology of PDLC doped with different concentrations of solvent green 28: (A0) 0 wt%; (B1) 0.3 wt%; (B2) 0.5 wt%; (B3) 0.8 wt%; (B4) 1.0 wt%; (B5) 1.5 wt%; (B6) 2.0 wt%. (The arrow points to the mesh of PDLC films.)

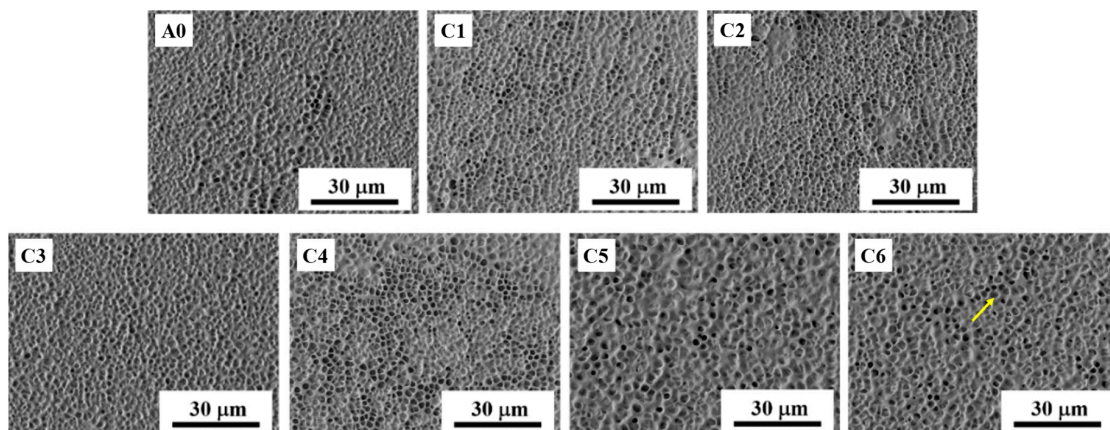


**Figure 5.** Microscopic morphology of PDLC doped with different concentrations of solvent blue 104: (A0) 0 wt%; (C1) 0.3 wt%; (C2) 0.5 wt%; (C3) 0.8 wt%; (C4) 1.0 wt%; (C5) 1.5 wt%; (C6) 2.0 wt%. (The arrow points to the mesh of PDLC films.)

### 3.3. Effect of Different Dyes and Their Doping Content on the Electro-Optical Performance of PDLC Dimming Film

Figure 6 shows the variation of transmittance with voltage and the effect of dye doping concentration on  $V_{th}$  and  $V_{sat}$  for different DDPDLC. As shown in Figure 6a,c,e, with the increase in dye concentration, the light absorption increases gradually, and the  $T_{on}$  of DDPDLC shows a trend of a gradual decrease in different degrees. The maximum absorption wavelengths of light for solvent red 111, solvent green 28 and solvent blue 104 are 550 nm, 560 nm~650 nm and 630 nm~710 nm, respectively, solvent red 111 absorbs less light at 632 nm; thus, solvent green 28 and solvent blue 104 can pass through PDLC films with even less light. Therefore, the  $T_{on}$  decreased less after the introduction of the red anthraquinone dye in the PDLC films system compared to the undoped sample A0.

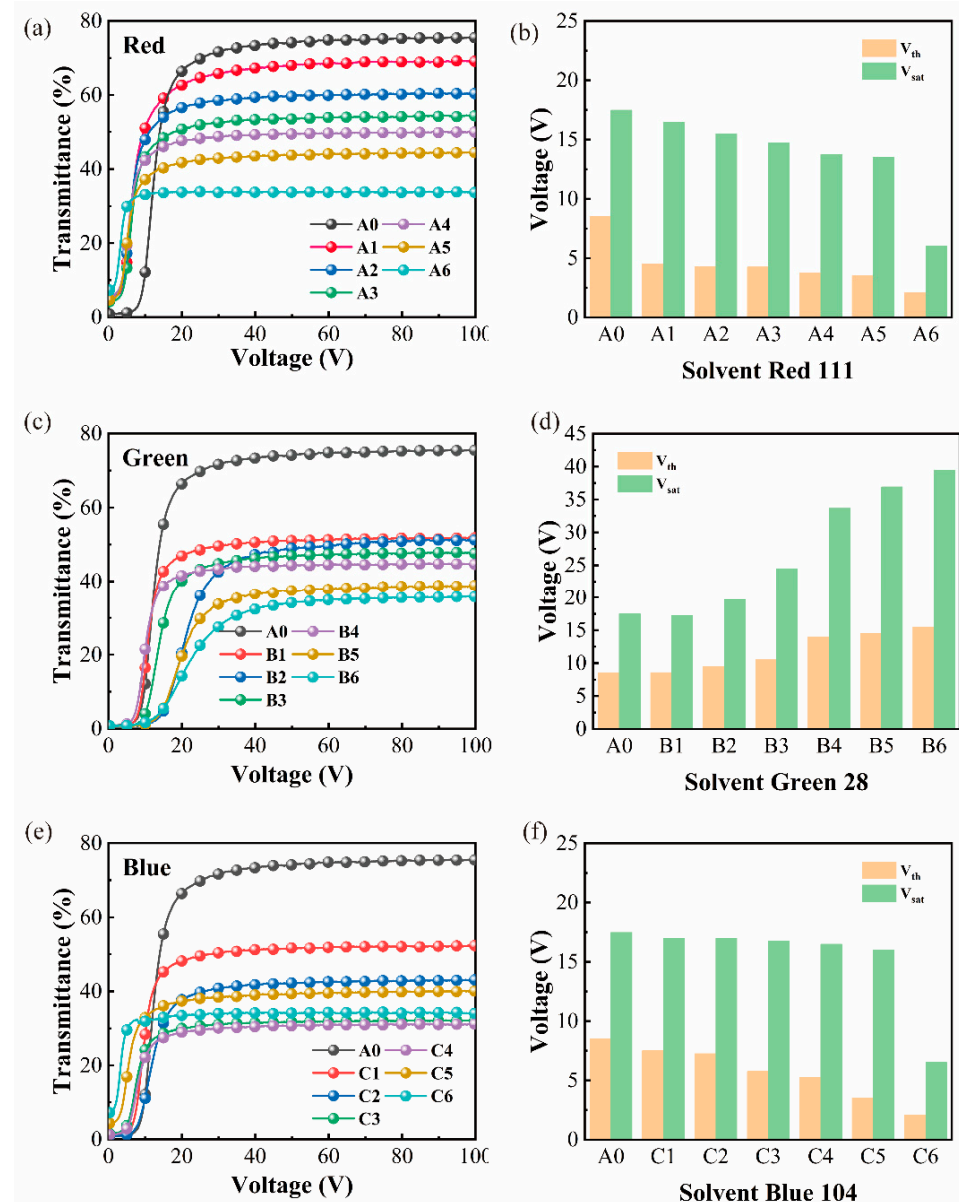


**Figure 6.** Electro-optical properties of DDPDLC: (a) The transmittance-voltage curves of solvent red 111; (b) The  $V_{th}$ ,  $V_{sat}$  of solvent red 111; (c) The transmittance-voltage curves of solvent green 28; (d) The  $V_{th}$ ,  $V_{sat}$  of solvent green 28; (e) The transmittance-voltage curves of solvent blue 104; (f) The  $V_{th}$ ,  $V_{sat}$  of solvent blue 104.

As shown in Figure 6b,f, PDLC films doped with solvent red 111 and solvent blue 104 dyes exhibit a reduction in driving voltages. This is because high dye concentration will increase the contact surface between the liquid crystal molecules and the polymer matrix, thus decreasing the polymeric matrix's capacity to bind liquid crystal molecules. As a result, the liquid crystal molecules can be driven easier, so  $V_{th}$  and  $V_{sat}$  are reduced. The results for solvent green 28 dyes are different from those of the other two dyes. According to Figure 6d, the  $V_{th}$  and  $V_{sat}$  increase as dye concentration rises. This is because liquid crystal droplet size gradually decreases, which is consistent with the SEM observations.

Figure 7 shows the effect of dye concentration variations on  $t_{on}$ ,  $t_{off}$  and CR, and it can be seen that the CR changes for different dye concentrations. From Figure 7a, it could be found that the contrast decreases with increasing dye concentration. Following the dye's incorporation into the polymerization process, some of it is present as liquid crystal droplets and the remainder is spread throughout the polymer matrix. The dye molecules in the liquid crystal microdroplet will be impacted by the electric field and oriented in the same direction as the liquid crystal when a voltage is applied to the PDLC film. The dichroic anthraquinone dye molecules in the polymer matrix will not be affected by the external magnetic field, so both  $T_{on}$  and  $T_{off}$  will be reduced. The variance of CR is primarily determined by the magnitudes of  $T_{on}$  and  $T_{off}$ . The main cause of the decline in CR for solvent red 111 and solvent blue 104 is that  $T_{on}$  has undergone a greater fall than  $T_{off}$ , as shown in Figure 6a,e. In contrast, the CR of solvent green 28 diminishes mostly because of the greater molecular size, which permits more light transmission through the polymer matrix and consequently increases  $t_{off}$  and because the  $t_{off}$  rises more than  $t_{on}$  falls, which eventually leads to a decrease in CR, as shown in Figure 6c.

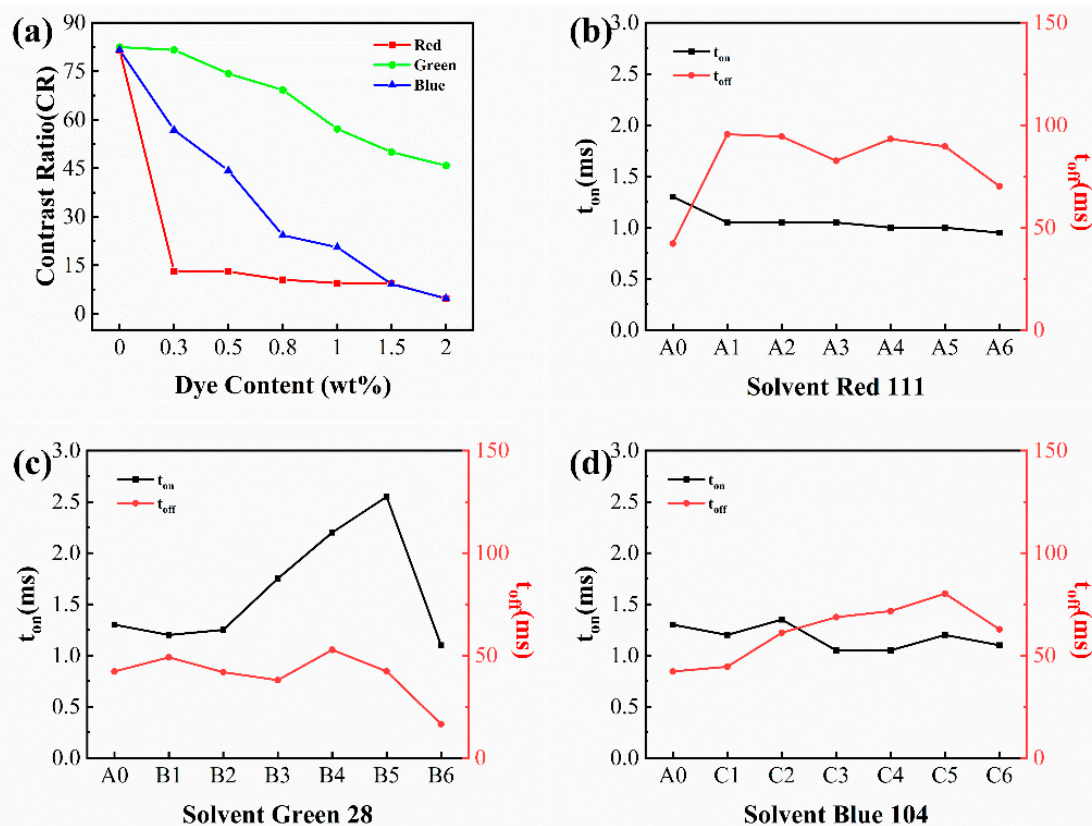


**Figure 7.** Electro-optical properties of DDPDLC: (a) The curve of CR and concentration; (b) The response time of solvent red 111; (c) The response time of solvent green 28; (d) The response time of blue 104.

The descending of  $T_{on}$  is more severe than the ascending of  $T_{off}$ , so the CR gradually decreases, as seen in Figure 6c. Figure 7b–d demonstrate the  $t_{on}$  and  $t_{off}$  trends for all samples with reaction times less than 150.0 ms. It is shown that the anthraquinone dye addition has no effect on the typical reaction threshold of PDLC films.

### 3.4. Effect of Different Dyes and Their Doping Content on Haze and Transmittance of PDLC Film

Figure 8a shows the variation of haze and transmittance with concentration for solvent red 111. The DDPDLC haze decreased and then increased with increasing dye concentration, reaching a minimum value at sample A3 at 0.8 wt% dye concentration. The doping of the dye molecules intercalates into the LC polymer to increase the mesh size, matching the refractive index between the substrate and the LC molecules, resulting in smaller haze. On the other hand, when the dye molecules continue to be added to a certain extent, some of the dye molecules are no longer able to enter the network structure of the LC polymer, and the dye molecules out of the network will increase the refractive index and make the haze show a tendency to increase. The effect of the stacked dye molecules is greater than the effect of mesh size on the refractive index on the refractive index, and the combined effect makes the haze increase.

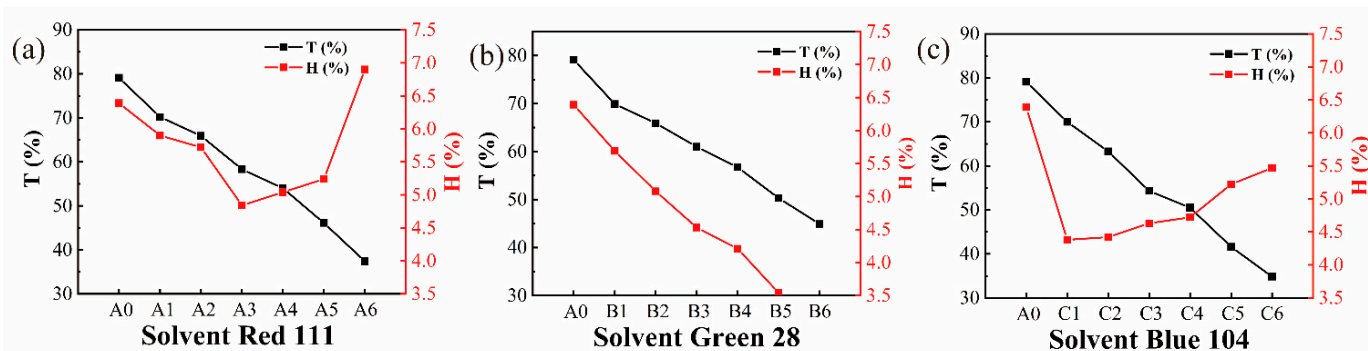


**Figure 8.** The haze and transmittance of DDPDLC: (a) solvent red 111; (b) solvent green 28 (c) solvent blue 104.

Figure 8b demonstrates the change of solvent green 28's haze and transmittance with dye concentration. As can be seen from the figure, when the dye concentration rises, both haze and transmittance decrease. This is due to the large size of the dye molecule, which results in a "light leaking" phenomenon that lowers the film's transmittance and gradually diminishes the haze. Figure 8c shows the trend of solvent blue 104, which is formed for the same reason as in solvent red 111.

### 3.5. Effect of Different Dyes and Their Doping Contents on the Mechanical Properties of PDLC Films

Figure 9 illustrates the mechanical properties of DDPDLC, and it can be seen that the shear force decreases with increasing dye content. The introduction of the dye causes an increase in impurities in the polymerization system, which causes the mechanical characteristics to progressively deteriorate as dye concentration rises. A portion of the light is absorbed by the dye, which then dyes decomposes, impairing the matrix's ability to polymerize and lowering its mechanical characteristics [50,52].

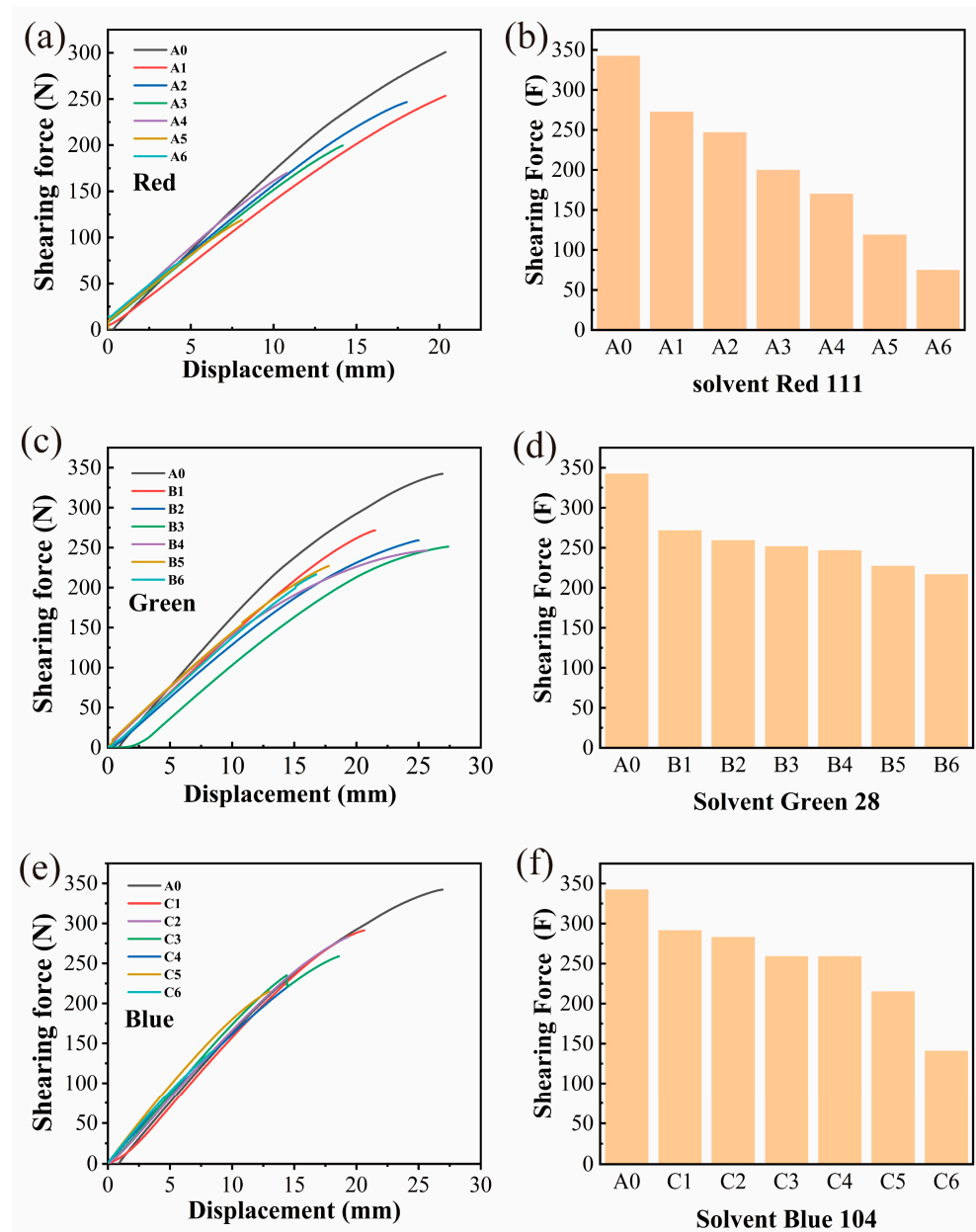


**Figure 9.** Mechanical properties of DDPDLC, shearing Force-Displacement curve and Shearing Force curve: (a) The shearing Force-Displacement curve of solvent red 111; (b) The shearing Force-Displacement curve of solvent green 28; (c) The shearing Force-Displacement curve of solvent blue 104; (d) The Shearing Force curve of solvent red 111; (e) The Shearing Force curve of solvent green 28; (f) The Shearing Force curve of solvent blue 104.

#### 4. Conclusions

In this comparative study, it has been investigated how various dyes and their doping concentrations affected the network morphology, electro-optical characteristics, haze, transmittance, and mechanical properties of PDLC films. The mesh size of solvent red 111 and solvent blue 104 doped PDLC films increased gradually as the dye concentration increased.  $V_{th}$ ,  $V_{sat}$ , CR and transmittance all gradually decreased. The haze first decreased and then increased, reaching the lowest levels at 0.8 wt% and 0.3 wt%, respectively. The mesh size increases and then decreases as the concentration of solvent green 28 increases, and the mesh distribution becomes denser. The  $V_{th}$  and  $V_{sat}$  gradually increased, and CR gradually decreased. The haze and open-state transmittance decreased gradually as the content increased, and the haze was lowest when the doping content was 2.0 wt%.

The dye increased the impurities of the polymer, resulting in a decrease in mechanical properties for all DDPDLCs. Moreover, the insertion of the dyes has a minimal impact on the switching response time of PDLC films, which could be controlled within 150 ms. The effect of haze on the gamut range was significant, and in order to make DDPDLC films more suitable for military camouflage, more environmentally friendly films were prepared. When the dye doping concentrations of solvent red 111, solvent green 28 and solvent blue 104 were 0.8 wt%, 2.0 wt% and 0.3 wt%, respectively, corresponding to their best performance. This study provides a basis for exploring the application of color-changing PDLC films in military camouflage applications.

**Author Contributions:** Conceptualization, C.Z. (Chenghu Zhao) and Y.G.; methodology, C.Z. (Chenghu Zhao) and M.Y.; validation, Y.H., C.Z. (Cheng Zou) and Y.G.; investigation, C.Z. (Chenghu Zhao) and J.X.; resources, J.X. and Y.H.; data curation, C.Z. (Chenghu Zhao); writing—original draft preparation, C.Z. (Chenghu Zhao); writing—review and editing, C.Z. (Chenghu Zhao) and Y.G.; supervision, Y.G. and H.Y.; funding acquisition, C.Z. (Cheng Zou), Q.W., M.Y. and Y.G. All authors have read and agreed to the published version of the manuscript.

**Funding:** This work was supported by the National Natural Science Foundation of China [51921002, 51927806, 52103071, 52203322, 52073081, 52203322]; the National Key R&D Program of China [2022YFB3603703].

**Conflicts of Interest:** The authors declare no conflict of interest.

## References

1. Han, T.; Bai, X.; Thong, J.T.; Li, B.; Qiu, C.W. Full control and manipulation of heat signatures: Cloaking, camouflage and thermal metamaterials. *Adv. Mater.* **2014**, *26*, 1731–1734. [[CrossRef](#)]
2. Xu, C.; Stiubianu, G.T.; Gorodetsky, A.A. Adaptive infrared-reflecting systems inspired by cephalopods. *Science* **2018**, *359*, 1495–1500. [[CrossRef](#)] [[PubMed](#)]
3. Caffarri, S.; Broess, K.; Croce, R.; van Amerongen, H. Excitation Energy Transfer and Trapping in Higher Plant Photosystem II Complexes with Different Antenna Sizes. *Biophys. J.* **2011**, *100*, 2094–2103. [[CrossRef](#)]
4. Kindervater, K.H. The emergence of lethal surveillance: Watching and killing in the history of drone technology. *Secur. Dialogue* **2016**, *47*, 223–238. [[CrossRef](#)]
5. Shimoni, M.; Haelterman, R.; Perneel, C. Hypersectral Imaging for Military and Security Applications: Combining Myriad Processing and Sensing Techniques. *IEEE Geosci. Remote Sens. Mag.* **2019**, *7*, 101–117. [[CrossRef](#)]
6. Deng, Z.; Su, Y.; Qin, W.; Wang, T.; Wang, X.; Gong, R. Nanostructured Ge/ZnS Films for Multispectral Camouflage with Low Visibility and Low Thermal Emission. *ACS Appl. Nano Mater.* **2022**, *5*, 5119–5127. [[CrossRef](#)]
7. Pimenta, C.; Morais, C.; Figueiro, R. Thermal camouflage clothing in diurnal and nocturnal environments. In *Key Materials*; Trans Tech Publications Ltd.: Stafa-Zurich, Switzerland, 2021; pp. 37–43.
8. Zhang, Y.; Chen, J.; Shen, L. Hybrid hierarchical trajectory planning for a fixed-wing UCAV performing air-to-surface multi-target attack. *J. Syst. Eng. Electron.* **2012**, *23*, 536–552. [[CrossRef](#)]
9. A thin radar-infrared stealth-compatible structure: Design, fabrication, and characterization. *Chin. Phys. B* **2014**, *23*, 025201. [[CrossRef](#)]
10. Zhong, S.; Wu, L.; Liu, T.; Huang, J.; Jiang, W.; Ma, Y. Transparent transmission-selective radar-infrared bi-stealth structure. *Opt. Express* **2018**, *26*, 16466–16476. [[CrossRef](#)]
11. Mischiati, M.; Krishnaprasad, P.S. The dynamics of Mutual Motion Camouflage. *Syst. Control. Lett.* **2012**, *61*, 894–903. [[CrossRef](#)]
12. Dou, S.; Xu, H.; Zhao, J.; Zhang, K.; Li, N.; Lin, Y.; Pan, L.; Li, Y. Bioinspired microstructured materials for optical and thermal regulation. *Adv. Mater.* **2021**, *33*, 2000697. [[CrossRef](#)]
13. Wang, G.; Chen, X.; Liu, S.; Wong, C.; Chu, S. Mechanical Chameleon through Dynamic Real-Time Plasmonic Tuning. *ACS Nano* **2016**, *10*, 1788–1794. [[CrossRef](#)]
14. Yoshioka, S.; Matsuhana, B.; Tanaka, S.; Inouye, Y.; Oshima, N.; Kinoshita, S. Mechanism of variable structural colour in the neon tetra: Quantitative evaluation of the Venetian blind model. *J. R. Soc. Interface* **2011**, *8*, 56–66. [[CrossRef](#)] [[PubMed](#)]
15. Sung, G.-F.; Wu, P.-C.; Zyryanov, V.Y.; Lee, W. Electrically active and thermally passive liquid-crystal device toward smart glass. *Photon Res.* **2021**, *9*, 2288–2295. [[CrossRef](#)]
16. Gu, C.; Jia, A.-B.; Zhang, Y.-M.; Zhang, S.X.-A. Emerging Electrochromic Materials and Devices for Future Displays. *Chem. Rev.* **2022**, *122*, 14679–14721. [[CrossRef](#)] [[PubMed](#)]
17. Nasir, N.; Kumar, S.; Kim, M.; Nguyen, V.H.; Suleman, M.; Park, H.M.; Lee, S.; Kang, D.; Seo, Y. Effect of the Photoinitiator Concentration on the Electro-optical Properties of Thiol-Acrylate-Based PDLC Smart Windows. *ACS Appl. Energy Mater.* **2022**, *5*, 6986–6995. [[CrossRef](#)]

18. Song, R.; Li, G.; Zhang, Y.; Rao, B.; Xiong, S.; He, G. Novel electrochromic materials based on chalcogenoviologens for smart windows, E-price tag and flexible display with improved reversibility and stability. *Chem. Eng. J.* **2021**, *422*, 130057. [[CrossRef](#)]
19. Villabona, M.; Benet, M.; Mena, S.; Al-Kaysi, R.O.; Hernando, J.; Guirado, G. Multistimuli-responsive fluorescent switches based on spirocyclic meisenheimer compounds: Smart molecules for the design of optical probes and electrochromic materials. *J. Org. Chem.* **2018**, *83*, 9166–9177. [[CrossRef](#)]
20. Onaka, J.; Iwase, T.; Fukui, M.; Koyama, D.; Matsukawa, M. Ultrasound liquid crystal lens with enlarged aperture using traveling waves. *Opt. Lett.* **2021**, *46*, 1169–1172. [[CrossRef](#)]
21. Bronnikov, S.; Kostromin, S.; Zuev, V. Polymer-dispersed liquid crystals: Progress in preparation, investigation, and application. *J. Macromol. Sci. Part B* **2013**, *52*, 1718–1735. [[CrossRef](#)]
22. Ailincal, D.; Marin, L. Eco-friendly PDLC composites based on chitosan and cholesteryl acetate. *J. Mol. Liq.* **2021**, *321*, 114466. [[CrossRef](#)]
23. Bouteiller, L.; Barny, P.L. Polymer-dispersed liquid crystals: Preparation, operation and application. *Liq. Cryst.* **1996**, *21*, 157–174. [[CrossRef](#)]
24. Torres-Cisneros, M.; LiKamWa, P.; May-Arrijo, D.; Ibarra-Manzano, O.; Plascencia-Mora, H.; Aguilera-Gómez, E.; Aviña-Cervantes, J.G.; Sanchez-Mondragon, J.J.; Song, Q.; Andrade-Lucio, J.A.; et al. Nano-droplet formation in polymer dispersed liquid crystals. *Phys. Status Solidi C* **2012**, *9*, 1515–1520. [[CrossRef](#)]
25. Kim, M.; Park, K.J.; Seok, S.; Ok, J.M.; Jung, H.-T.; Choe, J.; Kim, D.H. Fabrication of Microcapsules for Dye-Doped Polymer-Dispersed Liquid Crystal-Based Smart Windows. *ACS Appl. Mater. Interfaces* **2015**, *7*, 17904–17909. [[CrossRef](#)]
26. Xu, J.; Yu, M.; Chen, G.; Wang, X.; Hu, J.; Zou, C.; Wang, Q.; Xiao, J.; Gao, Y.; Zhu, S.; et al. Study on the preparation and performance of an electrically controlled dimming film with wide working temperature range. *J. Mol. Liq.* **2022**, *367*, 120408. [[CrossRef](#)]
27. Gong, S.; Cao, Y.; Fang, X.; Wang, Y.; Liu, Q.; Gui, H.; Shen, C.; Cao, X.; Kim, E.S.; Zhou, C. Carbon Nanotube Macroelectronics for Active Matrix Polymer-Dispersed Liquid Crystal Displays. *ACS Nano* **2016**, *10*, 10068–10074.
28. Wang, P.-C.; MacDiarmid, A.G. Integration of polymer-dispersed liquid crystal composites with conducting polymer thin films toward the fabrication of flexible display devices. *Displays* **2007**, *28*, 101–104. [[CrossRef](#)]
29. Ma, L.; Li, C.; Sun, L.; Song, Z.; Lu, Y.; Li, B. Submicrosecond electro-optical switching of one-dimensional soft photonic crystals. *Photon Res.* **2022**, *10*, 786–792. [[CrossRef](#)]
30. Ishinabe, T.; Horii, Y.; Shibata, Y.; Fujikake, H. Light distribution control of layer-structured PDLC fabricated by using micro lens structure and anisotropically diffused UV light. *Opt. Express* **2019**, *27*, 13416–13429. [[CrossRef](#)]
31. Sheeta, G.H.; Liu, Q.; Senyuk, B.; Fleury, B.; Smalyukh, I.I. Electric switching of visible and infrared transmission using liquid crystals co-doped with plasmonic gold nanorods and dichroic dyes. *Opt. Express* **2018**, *26*, 22264–22272. [[CrossRef](#)]
32. Chen, Y.; Zhang, Y.; Li, H.; Li, Y.; Zheng, W.; Quan, Y.; Cheng, Y. Dynamic Circularly Polarized Luminescence with Tunable Handedness and Intensity Enabled by Achiral Dichroic Dyes in Cholesteric Liquid Crystal Medium. *Adv. Mater.* **2022**, *34*, 2202309. [[CrossRef](#)] [[PubMed](#)]
33. Gahotra, R.; Sharma, V.; Dogra, A.R.; Malik, P.; Kumar, P. Performance augmentation of bistable cholesteric liquid crystal light shutter- effect of dichroic dye on morphological and electro-optical characteristics. *Opt. Mater.* **2022**, *127*, 112243. [[CrossRef](#)]
34. Fegan, S.K.; Kirsch, P.; Müller-Plathe, F. The alignment of dichroic dyes in a nematic liquid crystal: A molecular dynamics investigation. *Liq. Cryst.* **2018**, *45*, 1377–1384. [[CrossRef](#)]
35. Kumar, P.; Sharma, V.; Jaggi, C.; Malik, P.; Raina, K.K. Orientational control of liquid crystal molecules via carbon nanotubes and dichroic dye in polymer dispersed liquid crystal. *Liq. Cryst.* **2017**, *44*, 843–853. [[CrossRef](#)]
36. Shibata, Y.; Maruyama, S.; Ishinabe, T.; Matsumoto, Y.; Fujikake, H. Polarization characteristics of single-crystalline dichroic azo dye grown in nematic-phase liquid crystal. *JPN. J. Appl. Phys.* **2021**, *60*, 081001. [[CrossRef](#)]
37. Chatterjee, S.; Kumar, G.S. Binding of fluorescent acridine dyes acridine orange and 9-aminoacridine to hemoglobin: Elucidation of their molecular recognition by spectroscopy, calorimetry and molecular modeling techniques. *J. Photochem. Photobiol. B Biol.* **2016**, *159*, 169–178. [[CrossRef](#)] [[PubMed](#)]
38. Sun, H.T.; Xie, Z.P.; Ju, C.; Hu, X.W.; Yuan, D.; Zhao, W.; Shui, L.; Zhou, G. Dye-Doped Electrically Smart Windows Based on Polymer-Stabilized Liquid Crystal. *Polymers* **2019**, *11*, 694. [[CrossRef](#)]
39. Onsal, G.; Kocakulah, G.; Kahyaoglu, A.; Koysal, O. Influence of azo dye concentration on dielectric response in polymer dispersed liquid crystal composites. *J. Mol. Liq.* **2019**, *284*, 607–615. [[CrossRef](#)]
40. Ahmad, F.; Jamil, M.; Jeon, Y.J. New developments in the dye-doped polymer dispersed liquid crystals gratings: A review. *Int. J. Polym. Anal. Charact.* **2017**, *22*, 659–668. [[CrossRef](#)]
41. Mhatre, M.M.; Katariya-Jain, A.; Deshmukh, R.R. Enhancing morphological, electro-optical and dielectric properties of polymer-dispersed liquid crystal by doping of disperse Orange 25 dye in LC E7. *Liq. Cryst.* **2022**, *49*, 790–803. [[CrossRef](#)]
42. Malik, P.; Raina, K.K. Dichroic dye-dependent studies in guest-host polymer-dispersed liquid crystal films. *Phys. B-Condens. Matter.* **2010**, *405*, 161–166. [[CrossRef](#)]
43. Katariya-Jain, A.; Deshmukh, R.R. Effects of dye doping on electro-optical, thermo-electro-optical and dielectric properties of polymer dispersed liquid crystal films. *J. Phys. Chem. Solids* **2022**, *160*, 110363. [[CrossRef](#)]
44. An, S.; Ling, J.; Gao, Y.; Xiao, Y. Effects of varied ionic calcium and phosphate on the proliferation, osteogenic differentiation and mineralization of human periodontal ligament cells in vitro. *J. Periodontal Res.* **2012**, *47*, 374–382. [[CrossRef](#)] [[PubMed](#)]

45. Hu, J.; Hu, W.; Zhang, S.; Sun, C.; Lan, R.; Cao, Y.; Ren, Y.; Xu, J.; Wang, X.; Saeed, M.H.; et al. Combined effect of hydroxylated and fluorinated acrylate monomers on improving the electro-optical and mechanical performances of PDLC-films. *Liq. Cryst.* **2022**, *49*, 769–779. [[CrossRef](#)]
46. Yu, M.; Xu, J.; Wang, T.; Zhang, L.; Wei, H.; Zou, C.; Gao, Y.; Yang, H. Effects of acrylate monomers with different alkyl chain structure on the electro-optical properties and microstructure of polymer dispersed liquid crystals. *J. Appl. Polym. Sci.* **2022**, *139*, e53056. [[CrossRef](#)]
47. Debije, M.G.; Menelaou, C.; Herz, L.M.; Schenning, A.P. Combining positive and negative dichroic fluorophores for advanced light management in luminescent solar concentrators. *Adv. Opt. Mater.* **2014**, *2*, 687–693. [[CrossRef](#)]
48. Sharma, V.; Kumar, P.; Sharma, A.; Raina, K.K. Droplet configuration control with orange azo dichroic dye in polymer dispersed liquid crystal for advanced electro-optic characteristics. *J. Mol. Liq.* **2017**, *233*, 122–130. [[CrossRef](#)]
49. Kumar, P.; Sharma, V.; Jaggi, C.; Raina, K.K. Dye-dependent studies on droplet pattern and electro-optic behaviour of polymer dispersed liquid crystal. *Liq. Cryst.* **2017**, *44*, 757–767. [[CrossRef](#)]
50. Deshmukh, R.R.; Katariya Jain, A. The complete morphological, electro-optical and dielectric study of dichroic dye-doped polymer-dispersed liquid crystal. *Liq. Cryst.* **2014**, *41*, 960–975. [[CrossRef](#)]
51. Jayoti, D.; Malik, P.; Singh, A. Analysis of morphological behaviour and electro-optical properties of silica nanoparticles doped polymer dispersed liquid crystal composites. *J. Mol. Liq.* **2017**, *225*, 456–461. [[CrossRef](#)]
52. Zhang, C.; Wang, D.; Cao, H.; Song, P.; Yang, C.; Yang, H.; Hu, G.H. Preparation and electro-optical properties of polymer dispersed liquid crystal films with relatively low liquid crystal content. *Polym. Adv. Technol.* **2013**, *24*, 453–459. [[CrossRef](#)]

**Disclaimer/Publisher’s Note:** The statements, opinions and data contained in all publications are solely those of the individual author(s) and contributor(s) and not of MDPI and/or the editor(s). MDPI and/or the editor(s) disclaim responsibility for any injury to people or property resulting from any ideas, methods, instructions or products referred to in the content.